2009

Electrohydrodynamic instabilities in microchannels: a computational study

Shibi Vasisht Kapisthalam Vasudevan
Iowa State University

Electrohydrodynamic instabilities in microchannels: a computational study

by

Shibi Vasisht Kapisthalam Vasudevan

A thesis submitted to the graduate faculty

in partial fulfillment of the requirements for the degree of

MASTER OF SCIENCE

Major: Aerospace Engineering

Program of Study Committee:
Paul Durbin, Major Professor
Stephen Holland
Hui Hu

Iowa State University

Ames, Iowa

2009

DEDICATION

For Ammaji and Appaji

TABLE OF CONTENTS

LIST OF TABLES

LIST OF FIGURES

ACKNOWLEDGEMENTS

I would like to thank my advisor, Professor Paul Durbin. It was indeed a great honor to work with him. I benefitted immensely, not only due to his great knowledge and scholarship but also due to his kindness and general unassuming nature. He remains an inspiration for anything else I might do in life. I would also like to thank my committee members, Professor Hu and Professor Holland for kindly agreeing to be on my committee and for carefully reading my thesis. I would like to thank several friends who helped me out in the course of my studies and research at Iowa State. Jason Ryon helped me a lot in the initial parts of this work and Dr. Jongwook Joo provided a lot of guidance during the latter parts of this work. I would also like to thank the following people in no particular order: Mohammad Abrar Hasan, Haiyang Gao, Insu Chang, Dan Harper, Jason Busch, Sunil Arolla, Dr.Baskar Ganapathysubramaniam, Anand Gopakumar, Brandon Williams, Shourya Otta, Pallavi Padyala, Elbert Jeyapaul and Varun Vikas. I would like to thank my current and former friends at Iowa State, including, but not limited to, Prem, Vichu, Ganesh, Sriram, Nikhil and Niranjan. I am extremely grateful to the Aerospace Engineering department for being very generous in their financial support in the form of Teaching Assistantships and also for providing the computational resources for carrying out the simulations. I would like to thank the support staff of the Aerospace department, particularly the graduate secretary Ms. Dee Pfeiffer for taking care of all kinds of administrative requirements. I would also like to thank all the Professors under whom I took courses. I learnt a lot and had a lot of fun. At this point I would also like to thank my uncle Dr.Srikanth Padmanabhan who has been a great source of help and inspiration. Finally, I would like to thank my parents and my sister for their love and support throughout my entire life. I would like to dedicate this thesis to my parents.

ABSTRACT

A computational study is performed to study mixing characteristics in electrohydrodynamic flows at length scales of a micro-metre. A t-shaped microchannel is analyzed where two fluids of differing electrical conductivities are allowed to mix under the application of an external electric field. A two dimensional finite volume code based on the SIMPLE algorithm is employed. The effect of mixing is characterized in terms of a nondimensional parameter λ measuring the relative magnitude of the Coulombic force due to the electric field to the inertia force. Based on the relative concentrations of the two mixing streams a mixing efficiency is proposed and the mixing characteristics are studied by varying the value of the parameter λ(while keeping the concentration ratio fixed). Some observations regarding the time period of oscillation of the disturbance in the absence of any forcing are reported. Simulations are also performed by oscillating the applied external electric field to see the effect it has on the mixing compared to the case with the d.c. electric field. It was observed that oscillation of the electric field at the natural frequency significantly enhances the mixing quite in agreement with the general character of experimental observations. Simulation results for these different cases are presented.

CHAPTER 1. INTRODUCTION

1.1 Motivation

In an era of miniaturization of devices of engineering and biological interest, the control and manipulation of microfluidic devices assumes significance. Microfluidics may be defined as the control and manipulation of fluids when length scales are roughly of the order of 10^{-6} of a metre. Apart from several novel features of theoretical interest, these devices find extensive use in industrial applications. In the field of molecular biology, for example, microfluidic devices find use in DNA analysis: in polymerase chain reaction. They are also used as electroosmotic pumps for fuel cells. They are also extensively used in the fields of chemical analysis for micro total analysis sytems(μTAS)(Lin *et al* (2004)). These μTAS, allow the integration of several laboratory processes onto a single chip of only few millimetres in size. Several of these devices involve the flow of two or more fluids at different molar concentrations and the mixing, or lack of mixing, of the different fluids is of considerable interest. The proper functioning of these devices is dependent on the stability and mixing characteristics of the resultant flow. In certain cases we would like the flow to be stable, and the two streams to be unmixed, while in certain other cases we would prefer unstability of the resultant flow, primarily to generate significant mixing. For example isoelectric focussing devices depend on the stable transport of species while the opposite is true for micromixers, where significant mixing of the fluids is expected. Due to the small length scales involved, viscous damping plays a critical role in ensuring the stability of the resultant flow. Therefore, if we are looking to enhance mixing at such small length scales, several other means apart from molecular diffusion have to be explored. Various ways of enhancing mixing especially by supplying energy to the resultant devices are known and we shall concern ourselves with the case where mixing is achieved by means of an external applied

electric field. It is here that the experiments of Park *et al* (2005) and Chen and Santiago (2002) offer a lot of promise. They observed that when electric fields were applied orthogonal to the direction of the conductivity gradient, there exists a critical electric field beyond which the two streams mix together. Figures (1.1,1.2)from the experiments are reproduced below to give an idea of the kind of instability and mixing that can be achieved. This is an area broadly called electrohydrodynamics which also includes electrokinetics: the chief mechanism by which the instability is generated.(These terms are briefly reviewd in the section below). Following this Hu and Jin (2007) did a parametric study to quantify the mixing in a wide variety of electrokinetic configurations by varying the electric fields and concentration gradients. Several computational studies and studies of hydrodynamic stability were also conducted to further the understanding of these types of flow and the central ones amongst those are reviewed in a forthcoming section. Motivated by the various experiments, especially those performed by Hu and Jin (2007), the objective of the present study is to try to understand, through numerical simulations, the mixing characteristics in these t-shaped microchannels especially in the case where the external applied electric field is subject to oscillatory perturbations in contrast to the unforced case.

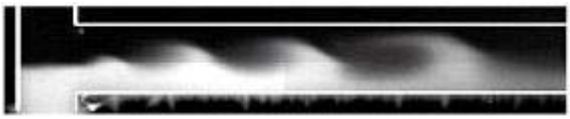

Figure 1.1 Instability in a T-shaped microchannel observed by Chen and Santiago (2002)

1.2 Some Technical Terms

In this section, the various terms associated with electrohydrodynamic phenomena are briefly reviewed. The exposition is largely based on Probstein (1994). Electrohydrodynamics(EHD), may be defined as the dynamics of electrically charged fluids. The following notions are useful in the study of EHD.

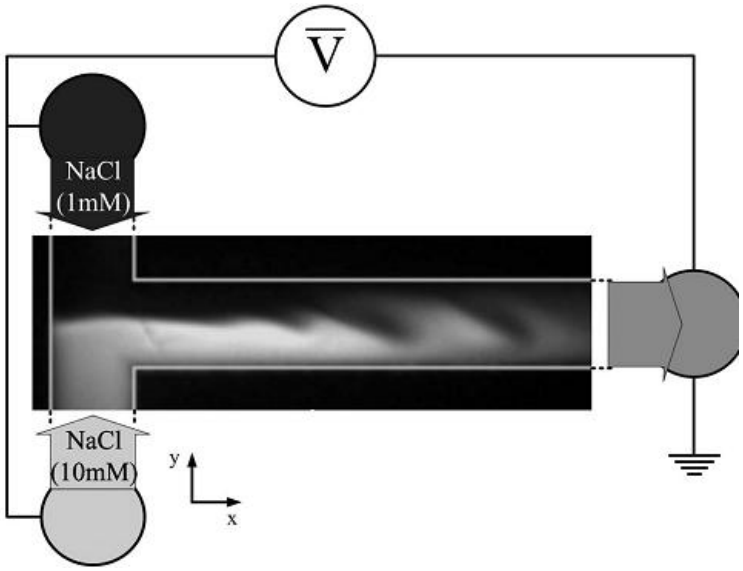

Figure 1.2 Instability in a T-shaped microchannel observed by Park *et al* (2005)

1.2.1 Electric Double Layer

When a solid surface is brought into contact with an aqueos medium, it acquires a surface electric charge, by means of various mechanisms such as ionization, ion adsorbtion and ion dissolution(see Probstein (1994)). The effect of this is that, when the charged surface comes into contact with an electrolyte solution which has charged ions, it will begin to influence the distribution of those ions. Oppositely charged ions(called counterions) will be attracted and ions of like charge(called coions)are repelled. When this is combined with the general mixing tendency because of the random thermal motion of the ions, it forms what is known as the *electric double layer*. This electrical double layer is located close to the charged surface and it results in redistributing the charged ions so that near the solid surface, there is an excess of counter ions compared to co-ions. The thickness of this diffuse charged double layer is characterized by the Debye length. For ions of a finite size the diffuse double layer is actually made of an inner layer called the Stern layer and an outer layer. The plane separating the two is called the Stern plane. (see Figure 1.3) The electric potential at this plane is close to the electrokinetic potential or the zeta (ζ) potential which is the electric potential at the shear

surface between the charged solid surface and the electrolyte solution. This shear surface is characterized as the plane where the mobile portion of the diffuse charged layer can slip or flow past the charge surface (Probstein (1994)). This motion of the electroosmotic velocity past a charged surface can be modelled using the Helmholtz-Smoluchowski equation given by

$$U = -\frac{\epsilon \zeta E}{\mu}$$

where μ is the viscosity of the fluid, E is the external applied electric field parallel to the solid wall surface, ϵ is the permittivity of the fluid and ζ is the zeta potential.

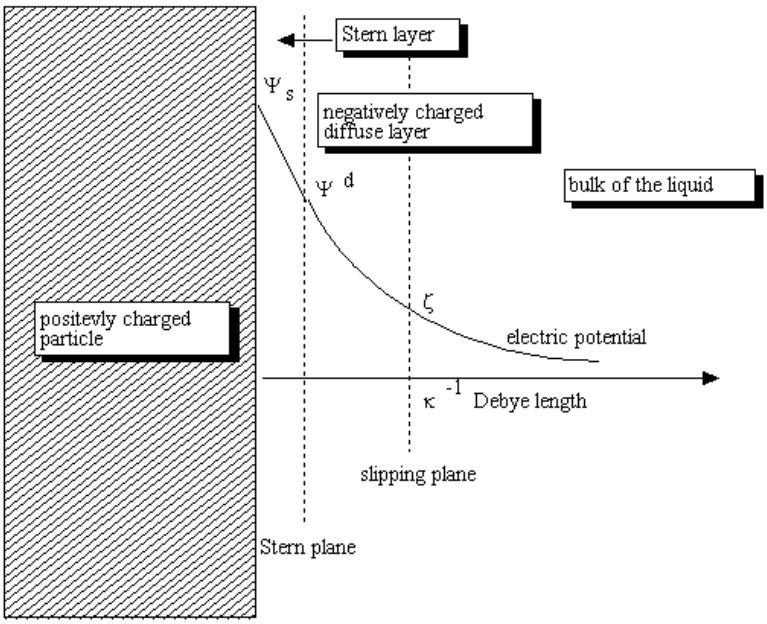

Figure 1.3 Electric double layer and associated potential. Picture taken from Double Layer (interfacial)

1.2.2 Electroosmosis and Electrophoresis

Electroosmosis may be defined as the movement of the liquid relative to a stationary charged surface. When an electric potential is applied to the double layer, the mobile portion of the double layer migrates towards the oppositely charged electrode(Oddy (2005)). This electromigration of the charged species causes viscous shearing of the adjacent liquid molecules resulting in bulk motion of the electrolyte. This motion may be modelled using the slip velocity de-

scribed above. Electrophoresis is the movement of a charged surface plus the attached material relative to a stationary liquid in an applied external electric field. (Probstein (1994))

1.2.3 Electrokinetics

We shall concern ourselves in this work with *electrokinetic phenomena*, which are due to the interactions of electric charges and liquids and are often characterized by the presence of an electic double layer(Oddy (2005)).The four phenomena which are classified as electrokinetic phenomena are (Probstein (1994)): electroosmosis, electrophoresis, streaming potential and sedimentation potential. The first two were discussed above while the last two are outside the scope of this work.

1.3 Survey of Literature

Electrohydrodynamics itself is a venerable old field, going as far back as the 17th century (Saville (1998)). It has been known, for quite some time, that electric fields, applied parallel or perpendicular to the direction of the conductivity gradient significantly affect stability and the mixing characteristics of the resultant flow. Several studies have been performed in this regard, some of which are reviewed below.One of the first comprehensive surveys of electrohydrodynamics was by Taylor and Melcher (1969). Their study was concerned with the interfacial deformation due to shear stesses of a parallel electric field applied to two fluids of different concentrations at rest. They showed that when a fluid system includes interfacial regions separated by fluids of different electrical properties, then the electromechanical coupling forces at the interface is likely to dominate the resulting electrohydrodynamics, i.e the surface interactions at the interface are very important. They presented several cases where cellular convection was achieved in a static liquid utilizing the electric shear forces. They also performed stability analysis on the instability due to the applied electric field(both a.c and d.c) on some characteristic flow configurations. Saville (1998) presents a derivation of the differential equations describing electrohydrodynamic flow. This model is called the leaky dielectric model which was first introduced by Taylor and Melcher (1969) The essence of the leaky dielectric

model is the Ohmic model in which the electrohydrodynamic instability is caused by the accumulation of charges at the material interfaces and it is then coupled to the fluid motion by means of electrical body forces. Also presented are experimental results on a wide class of electrohydrodynamic flows including the motion of charged drops, charged cylinders and apolar liquids showing qualitative agreement with the theory. Hoburg and Melcher (1976) looked at the problem of electric field applied perpendicular to the conductivity gradient, for which they performed a stability analysis. Chief among their findings was the fact that when the interface of the two fluids is modelled with a finite width, the flow exhibits instablity resulting in buckling and distortion of the interface. Baygents and Baldessari (1998) analysed the onset of electrohydrodynamic motion in a layer of liquid in which there is a continuous variation in the electrical conductivity, the conductivity gradients being associated with the gradients in the concentration of the charge carrying solutes. They performed a linear stability analysis and found that one relevent dimensionless parameter is an electric Rayleigh number Ra_e. The diffusion of conductivity is crucial to the existence of a critical electric field(depending on the above Rayleigh number) above which the flow is unstable. Chen *et al* (2005) looked at convective and absolute instabilities associated with conductivity gradients. They present experimental, analytical and computational results for the instability in a t-shaped microchannel. They used a model similar to the Ohmic model but allowed for two changes. They included a diffusive term for conductivity following Baygents and Baldessari (1998) and they neglected the charge relaxation process because of the extremely small time scale involved. Charge accumulation at the interfaces of conductivity gradients gives rise to forces causing instability. The electro-osmotic flow is also important. It plays a role in covecting the disturbance downstream unless it is offset by the electro-viscous velocity perturbation. Park *et al* (2005) presented several micromixer designs based on the observance of instabilities in t-shaped microchannels. They found that for a configuration with cavities in it, the Coulombic force due to the interaction of the charge that acumulates at the corners and the electric field leads to instability and increased mixing. Following this, Kang *et al* (2006) performed numerical analysis for the electroosmotic flow of two liquids with different concentrations in a t-shaped microchannel.

They showed that molecular diffusion played a critical role in instigating and maintaining the instability even without any external forcing. Furthermore, they also showed that molecular diffusion played a key role in making the wavy pattern look regular even though the flow was unstable. They also showed that the origin of the instability lies in the polarization induced by a conductivity gradient in the two mixing layers.

The present work is inspired for the most part by the experiments performed by Hu and Jin (2007). They looked at a wide variety of combinations of electric fields(both direct and alternating current) and concentration ratios. They quantified the mixing by proposing a notion of mixing efficiency. Central among their findings was the fact that for external forcing by means of an alternating electric field, the mixing is most enhanced when the frequency of the imposed electric field is the same as the shedding frequency of the convective waves when there is no forcing, i.e in the unforced natural oscillation case.

1.4 A brief overview of the instability mechanism

The basic nature of the instability process may be explained as follows. There is an accumulation of free charges at the interface due to diffusion of concentration and interface deformation. When an electric field is applied, this results in Coulombic forces acting in different directions which results in the generation of vortices which become unstable and propogate downstream when the applied electric field is above a certain threshold field. (Chen *et al* (2003) Kang *et al* (2006))

1.5 Scope of the current work

In this thesis, we look at the mixing of two liquids with similar mechanical properties but differing in their conductivity ratio,in a t-shaped microchannel in the presence of an external applied electric field. We would like to study the effect of forcing the external electric field and to see if this has any effect on the mixing for different values of the nondimensional parameter λ which may be described as the ratio of the Coulombic force to the inertia force(this is explained in the next chapter). A criteria of mixing is proposed and the effect of oscillating the electric

field on mixing is observed based on this criteria.

CHAPTER 2. NUMERICAL METHODS

2.1 Introduction

In this section the governing equations along with the boundary conditions are described. The discretization scheme and the algorithm used are also briefly discussed.

2.2 Governing Equations

Since electrohydrodynamic flow involves the application of an electric field, we need equations for both the fluid flow and the electric field and a way of coupling the two. The figure below represents the domain over which the analysis is going to take place. The following assumptions are made about the flow. The permittivity of the liquid is uniform. The electrolytes are free from chemical reaction. The activity coefficient is assumed to be unity. The thickness of the electrical double layer is insignificant compared to the length scales, which in this case is taken to be the channel width. These assumptions are consistent with previous experimental and theoretical work(Park *et al* (2005), Lin *et al* (2004))The electric double layer (Oddy (2005)) can be described as follows: When a solid phase comes in contact with an aqueous phase, the solid phase acquires a surface electric charge due to a variety of mechanisms. It also results in a thin diffuse charged layer near the surface. This thin charged layer is called the electric double layer(EDL). This electric double layer may be modeled as a slip velocity (Kang *et al* (2006)) which will be discussed later in this section.

In the electrostatic condition that governs the case we are considering, the simplified form of the Maxwell's equations are

$$\nabla \cdot (\varepsilon \mathbf{E}) = \rho_e \tag{2.1}$$

$$\nabla \times \mathbf{E} = 0 \tag{2.2}$$

$$\frac{\partial \rho_e}{\partial t} + \nabla \cdot \mathbf{i} = 0. \tag{2.3}$$

$\mathbf{E}$ is the electric field and ϕ is the electric potential and are related by the equation $\mathbf{E} = -\nabla\phi$. ε is the electrical permittivity, ρ_e is the free charge density, t is the time and $\mathbf{i}$ is the current density. For our purposes the electric current can be considered solely due to motion of the ions and diffusion and electromigration terms may be neglected. We then get the equation for the current as

$$\mathbf{i} = -\sigma\nabla\phi \tag{2.4}$$

where σ is the conductivity. σ is given by $\sigma = F^2(\omega_+ + \omega_-)c$ (Kang *et al* (2006)) and is proportional to the concentration c. In the absence of any chemical reation and because there is no new generation of ionic charges, the net charge must be conserved and we thus have the charge conservation equation.

$$\frac{\partial c}{\partial t} + \mathbf{u} \cdot \nabla c = D\nabla^2 c \tag{2.5}$$

where $D = 2D_+D_-/(D_+ + D_-)$ is the equivalent diffusivity. Because of the application of a DC electric field, the displacement current in equation 2.3, $\frac{\partial \rho_e}{\partial t}$ is neglected. Then the electric potential ϕ satisfies the following equation

$$\nabla \cdot (\sigma\nabla\phi) = 0 \tag{2.6}$$

Using the above equation and equation 2.1 we have the following equation for the free charge density.

$$\rho_e = -\frac{\varepsilon\nabla c \cdot \mathbf{E}}{c} \tag{2.7}$$

The momentum and continuity equations that govern an incompressible viscous (Newtonian) flow can be written as

$$\rho\frac{D\mathbf{u}}{Dt} = -\nabla p + \mu\nabla^2\mathbf{u} + \rho_e\mathbf{E} \tag{2.8}$$

$$\nabla \cdot \mathbf{u} = 0 \tag{2.9}$$

where, $\rho, \mathbf{u}, p, \mu$ are respectively the density, velocity, pressure and dynamic viscosity of the fluid under consideration and we have $\frac{D}{Dt} = \frac{\partial}{\partial t} + \mathbf{u}\cdot\nabla$. The extra term, $\rho_e\mathbf{E}$, in the momentum

equation is the force due to the electric field. We shall see that this term provides the necessary coupling between the flow field, electric potential and the equation governing the conservation of concentration.

2.3 Initial and Boundary Conditions

The domain of analysis is depicted in figure 2.1.

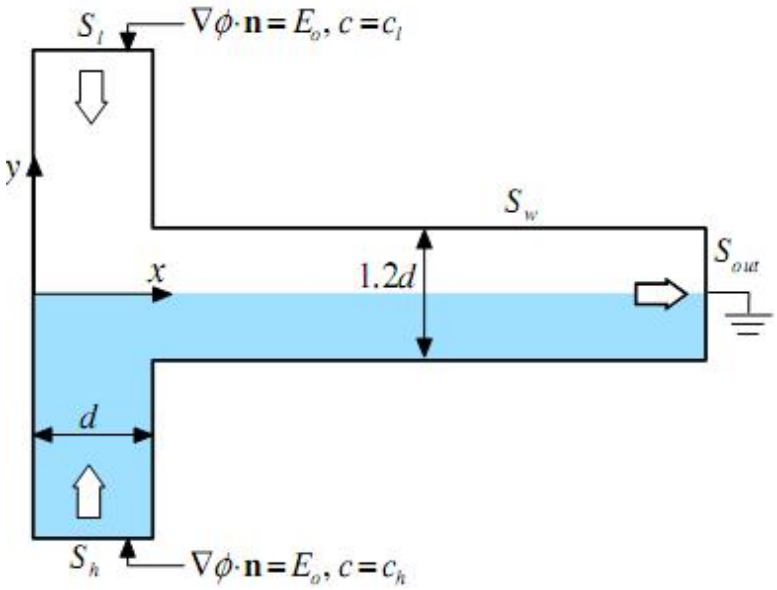

Figure 2.1 Domain of analysis from Kang *et al* (2006)

Using the thin electrical double layer assumption, we can model the electrical double layer as a slip velocity, called the Helmholtz-Smoluchowski slip velocity (Kang *et al* (2006)) , u_{HS}, as the slip velocity at the side walls, u_t

$$u_t = u_{HS} = -\frac{\varepsilon\zeta\mathbf{E}\cdot\mathbf{t}}{\mu} \tag{2.10}$$

here ζ is the zeta potential at the wall and $\mathbf{t}$ is the unit tangential vector on the wall. In the present work ad-hoc slip velocity is imposed on the boundaries, values for which were obtained using Park *et al* (2005). The boundary conditions used in the simulations were as follows, On the upper and lower walls, Upper wall:

$$c = c_l; \nabla\phi\cdot\mathbf{n} = E_o; u = 0, v = v_l \tag{2.11}$$

Lower wall:

$$c = c_h; \nabla\phi \cdot \mathbf{n} = E_o; u = 0, v = v_h \tag{2.12}$$

Side walls:

$$\nabla c \cdot \mathbf{n} = 0; \nabla\phi \cdot \mathbf{n} = 0; \mathbf{u} \cdot \mathbf{n} = 0, \mathbf{u} \cdot \mathbf{t} = u_{HS} \tag{2.13}$$

Outflow wall:

$$\nabla c \cdot \mathbf{n} = 0; \phi = 0; \frac{D\mathbf{u}}{Dt} = 0 \tag{2.14}$$

where c_h and c_l are the high and low concentrations of the two electrolytic liquids. E_o is the constant electric field applied at the inflow walls, $\mathbf{n}$ is the outward unit normal vector to the boundary walls.

2.4 Nondimensionalization

The following equations are used in order to non-dimensionalize the given equations The nondimensional time, lengths and velocities are given as

$$\bar{x} = \frac{x}{d} \tag{2.15}$$

$$\bar{y} = \frac{y}{d} \tag{2.16}$$

$$\bar{t} = \frac{t}{t_c} \tag{2.17}$$

$$\bar{\mathbf{u}} = \frac{\mathbf{u}}{\mathbf{u_c}} \tag{2.18}$$

The electric field, concentration, electric potential and the free charge density are nondimensionalized as follows,

$$\bar{\mathbf{E}} = \frac{\mathbf{E}}{E_o} \tag{2.19}$$

$$\bar{\phi} = \frac{\phi}{E_o d} \tag{2.20}$$

$$\bar{c} = \frac{c}{c_h - c_l} \tag{2.21}$$

$$\bar{\rho_e} = \frac{\rho_e}{\varepsilon(E_o/d)} \tag{2.22}$$

where the average inlet velocity is used as the characteristic velocity for nondimensionalization. The characteristic length scale, d, is the width of the channel at the inlet portion of the 'T',

i.e the width of the arms of the 'T'. The characteristic time scale is chosen as $t_c = \frac{d}{u_c}$. The reference electric field, E_o, is the constant electric field applied at the inlet. c_h and c_l are the higher and lower concentrations respectively, at the two inlets.

Using these nondimensional variables we obtain the following non-dimensional equations, where the overbar is not used to denote the nondimensional variables. Thus, from here onwards the variables and the equations are assumed to be dimensionless.

$$\frac{D\mathbf{u}}{Dt} = -\nabla p + \frac{1}{Re}\nabla^2\mathbf{u} + \lambda(\nabla^2\phi)\nabla\phi \tag{2.23}$$

$$\nabla \cdot (c\nabla\phi) = 0. \tag{2.24}$$

$$\frac{Dc}{Dt} = \frac{1}{Pe}\nabla^2 c \tag{2.25}$$

where $Re = \frac{u_c d}{\nu}$ is the Reynolds number. $Sc = \frac{\nu}{D}$ is the Schmidt number where D is the equivalent diffusivity, $Pe = \frac{u_c d}{D} = ReSc$ is the Peclet number which is the product of the Reynolds number and Schmidt number. The parameter λ , which is the ratio of the relative magnitude of the Coulombic force and the Inertia force is given by the following formula,

$$\lambda = \frac{\varepsilon {E_o}^2}{\rho {u_c}^2} \tag{2.26}$$

In the case we are considering we allow the Reynolds number to be 0.14, the Peclet number to be 87, the Schmidt number to be 622. The parameter λ will be varied during the course of the simulations to see the effect it has on the mixing characteristics.

2.5 Solution methodology

The differential form of the Navier Stokes equation(with the additional forcing term) is given below so as to facilitate easy reference during the description of the algorithm.

$$\frac{\partial(\rho u_i)}{\partial t} + \frac{\partial \rho u_i u_j}{\partial x_j} = \frac{\partial \tau_{ij}}{\partial x_j} - \frac{\partial p}{\partial x_i} + \lambda \frac{\partial^2 \phi}{\partial x_i^2}\frac{\partial \phi}{\partial x_i} \tag{2.27}$$

and the continuity equation,

$$\frac{\partial u_i}{\partial x_i} = 0$$

Here the second term in the left hand side of equation 2.27 is the convective part and the first equation in the right hand side is the viscous part. These equations are linearized (see ref. Ferziger and Peric (1994)) and we get the algebraic equations for the unknowns(velocities and pressure) of the form (the equation for velocity is given as an example)

$$A_P u_{i,P} + \sum_i A_l u_{i,l}^{n+1} = Q_{u_i}^{n+1} - (\frac{\delta p^{n+1}}{\delta x_i})$$

We shall follow the SIMPLE algorithm to discretize and solve the Navier Stokes equations. SIMPLE stands for Semi-Implicit Method for Pressure-Linked Equations and is described in detail by Patankar (1980) and also by Ferziger and Peric (1994). This method is a finite volume method, which means that the solution domain is divided into finite number of control volumes and across each of those volumes, the integral form of the conservation equations are solved. The centroid of the volumes has a computational node at which the variables of interest are stored. The advantage of this method is the fact that it is close to the physics of the flow as conservation equations are used at each of the smaller volumes. We use a collocated grid in which the same control volume is used for all the variables of interest.

The algorithm that is used is given below

1. Start the calculation at the new time step using the values at the old time step as an initial guess.

2. Assemble and solve the linearized algebraic equations so as to get the velocity components u_i^*

3. Solve a poisson equation to obtain the pressure correction term p'

4. Correct the pressure and velocity terms to get new velocities u_i which satisfy continuity equation and new pressure p

5. Solve the other equations for the electric potential ϕ and the concentration c

6. Use p as the new guessed pressure field p^* and repeat the previous steps until the corrections are very small.

A brief description of some of the steps in the algorithm is of order. The mass fluxes is given by, (here the "east" mass flux is given as an example)

$$\dot{m} = \int_{S_{i+1/2}} \rho \mathbf{v} \cdot \mathbf{n} dS \approx (\rho u)_{i+1/2} S_{i+1/2}$$

and the mass flux at the cell face is approximated using the central difference scheme $u_{i+1/2} = \frac{u(i+1,j)+u(i,j)}{2}$ Here S denotes the cell face area normal to the direction of the flow. The convective flux is given by,

$$F_{i+1/2} = \int_S \rho u_i \mathbf{v} \cdot \mathbf{n} dS = \dot{m}_{i+1/2} u_{i+1/2}$$

. Here, both a central difference scheme given by

$$F_{i+1/2} = \rho S \frac{u_i + u_{i+1}}{2}$$

and an upwind scheme which is given by

$$F_{i+1/2} = \begin{cases} \rho S u_i & \text{when } u_i > 0, \\ \rho S u_{i+1} & \text{when } u_i < 0. \end{cases}$$

are used in calculating the fluxes. Due to the blending scheme used, in the final analysis the upwind cancels out and we get a central scheme of second order. The coefficient for the viscous flux given by,

$$D = \frac{\mu S}{dx}$$

is implicitly is added to the coefficient matrix A. Since the terms involved in the convective derivative are nonlinear we linearlize it and, neglecting the higher order nonlinear terms obtain a Poisson equation for the pressure correction as (see Ferziger and Peric (1994))

$$\frac{\delta}{\delta x_i}(\frac{\delta \triangle p}{\delta x_i}) = (\frac{1}{\triangle t}) \frac{\delta(\rho u_i^*)}{\delta x_i} \tag{2.28}$$

And we use this pressure to update the velocity.

$$u_i^{n+1} = u_i^* - \frac{\triangle t}{\rho} \frac{\delta \triangle p}{\delta x_i} \tag{2.29}$$

Also in order to prevent the odd even decoupling because of a collocated grid arrangement, we use the Rhie and Chow interpolation (Rhie and Chow (1983)) to interpolate the fluxes using

four grid points so that any oscillations of the pressure field is taken into account. The same method is used to solve for the concentration c. Once the velocity field is known , then c is an unknown scalar and can be solved by the same methods of discretization, building up the matrix and then solving it. In order to solve the equation for ϕ the concentration c is used in the viscous flux term. The additional term in the momentum equations due to the electric field is simply added on as a body force source term. In order to implement boundary conditions, ghost cells were used. Thus, a new cell is artificially introduced beyond the boundary and the velocity at that cell is chosen so that in combination with the velocity at the first grid point in the domain, the required velocity at the boundary is satisfied by linearly interpolating the two velocities. The inflow, outflow and no slip boundary conditions were implemented using the ghost boundary condition. For example, for the no slip, the velocity at the ghost point is negative the velocity at the first grid point. For the pressure correction equation a zero gradient condition is imposed on all the boundaries where the mass flux is known, i.e the inflow, outflow and wall boundaries. The boundary conditions for electric potential and concentration are similarly imposed using the ghost cells and the same boundary conditions are used as is specified in Section 2.3 In order to solve the linearized equation the strongly implicit procedure developed by Stone (see Stone (1968)) is used. This is particularly suited to solve large systems of sparse matrices which are discretized from partial differential equations. This is known as the inner iterations where the entries in the coefficient matrices are fixed and it is solved by iteration to a specified degree of tolerance. We also integrate in time and set up the matrix at each time step. These are the outer iterations, which solves the equations is time for the unsteady case. Here an Euler implicit three-time level method is used so the values at the previous two time steps are used in the current time step calculation. A uniform cartesian grid of dimension 352×52 is used. The time step size is fixed at $\triangle t = 0.01$ The spatial discretisation used is $\triangle x = \triangle y = 0.04$ Because we use a cartesian grid, in order to generate the 'T' shape it was necessary to use "I-blanking". This consists of modifying the A matrix and the source terms SU, so that all the variables of interest are zeroed out in the

blanked region. This is implemented in the code as follows.

$$AP(I,J) = 1$$

$$SU(I,J) = 0$$

$$A_i(I,J) = 0$$

where i denotes all the neighbouring nodes with respect to the given node. This results in zeroing out all the variables of interest in the blanked out region. The boundary condition at the boundary of the rib is treated the same way using the ghost points which are simply shifted in their spatial locations compared to the unblanked regions. Two rectangular blanked regions are used in the current code to create the conditions of a 'T' shaped region. The code used is one that is available freely on the web (Ferziger and Peric ftp (1994)). A number of modifications to the existing code were made including conversion from Fortran 77 to Fortran 90, adding the equation for concentration, adding source term for the electric force, i-blanking the ribs to create a t shaped region and changing the inlet, outlet and boundary conditions.

CHAPTER 3. RESULTS: CASE I: UNFORCED CASE

In this chapter the simulation results for the case with a d.c electric field are presented. The value of λ is varied from 80 to 180 some of the salient features of the simulations are explored. We may recall that the parameter λ, measures the relative magnitude of the Coulombic force to the viscous force and increasing the value of this parameter is equivalent to increasing the electric field (and thereby the electric force) with respect to the viscous force.

3.1 Preliminary results

In this section we observe the results obtained by increasing the value of λ.

3.1.1 Case(i): $\lambda = 80$

The figures from the simulation are given below. These are contour plots of the concentrations of the two mixing streams. The blue regions are those with low concentrations and the red regions are those with a higher concentrations. As we can see from the figure, the instability generates a wavy pattern which grows initially but damps out as time progresses due to the dominant part played by the viscous forces.

3.1.2 Case(ii): $\lambda = 120$

In this case the wavy pattern generated does not die out after a period of time but sustains itself with some kind of periodicity. The strange pattern that came out of these simulations was that, associated with each value of λ was there was a natural frequency of oscillation of the mixing pattern(characterized here by monitoring the time evolution of the velocity at a single spatial point). This is explored in more detail the next section.

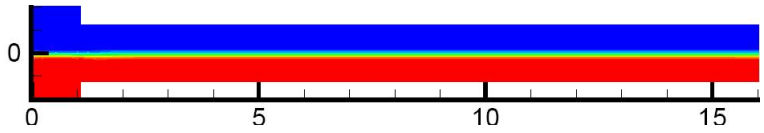

Figure 3.1 Plot of concentration, $\lambda = 80$, $t = 0.28$

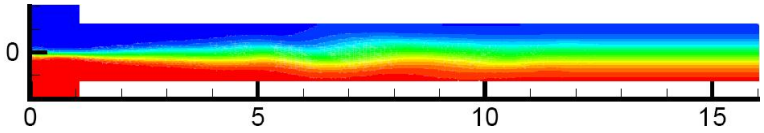

Figure 3.2 Plot of concentration, $\lambda = 80$, $t = 4.28$

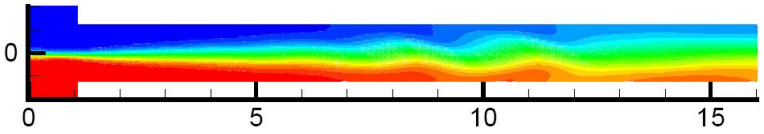

Figure 3.3 Plot of concentration, $\lambda = 80$, $t = 8.28$

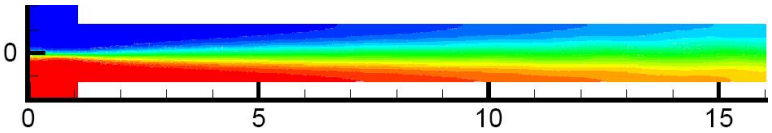

Figure 3.4 Plot of concentration, $\lambda = 80$, $t = 16.28$

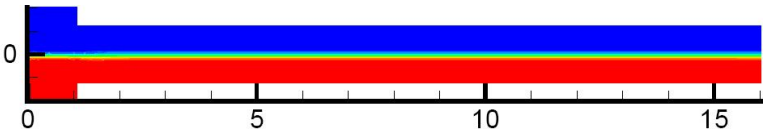

Figure 3.5 Plot of concentration, $\lambda = 120$, $t = 0.28$

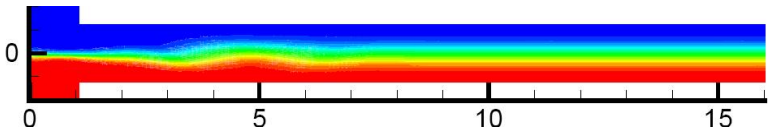

Figure 3.6 Plot of concentration, $\lambda = 120$, $t = 2.28$

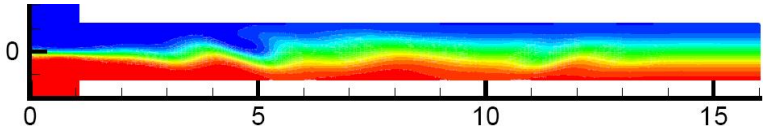

Figure 3.7 Plot of concentration, $\lambda = 120$, $t = 4.28$

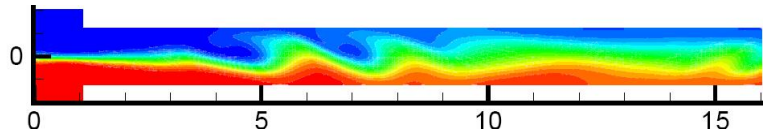

Figure 3.8 Plot of concentration, $\lambda = 120$, $t = 6.28$

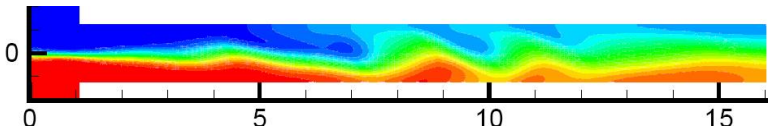

Figure 3.9 Plot of concentration, $\lambda = 120$, $t = 8.28$

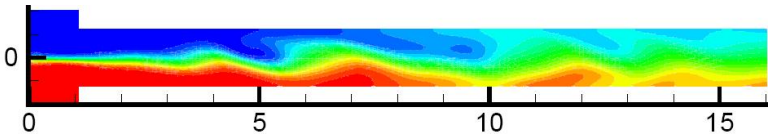

Figure 3.10 Plot of concentration, $\lambda = 120$, $t = 10.28$

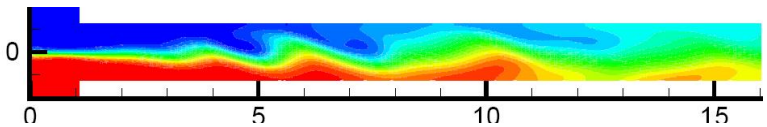

Figure 3.11 Plot of concentration, $\lambda = 120$, $t = 12.28$

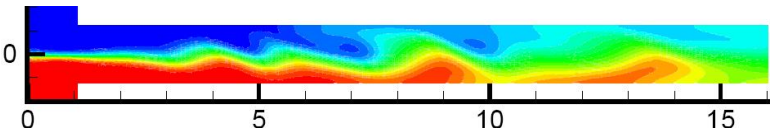

Figure 3.12 Plot of concentration, $\lambda = 120$, $t = 14.28$

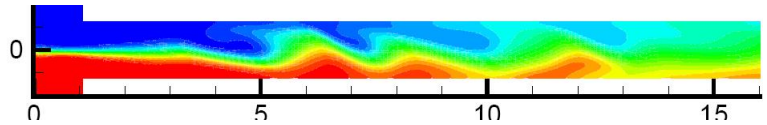

Figure 3.13 Plot of concentration, $\lambda = 120$, $t = 16.28$

3.1.3 Case(iii): $\lambda = 150$

In this section the value of lambda is increased to 150 . We can observe from the results that the mixing tends to increase with increase in the value of λ. One can also see the formation of a hump shaped region in Figure 3.19 and it propogates downstream.

3.1.4 Case(iv): $\lambda = 180$

The results of the simulation are given below. There are atleast three humps that appear and propogate downstream. It appears that there is a lot more mixing in this case based on looking at the pictures.

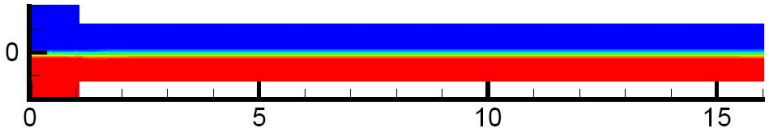

Figure 3.14 Plot of concentration, $\lambda = 150$, $t = 0.28$

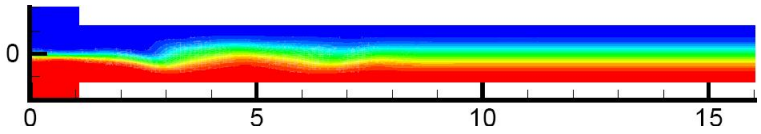

Figure 3.15 Plot of concentration, $\lambda = 150$, $t = 2.28$

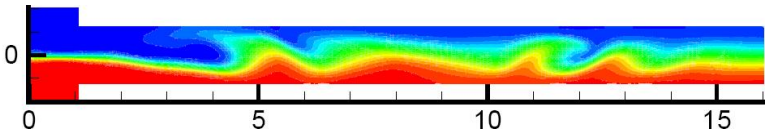

Figure 3.16 Plot of concentration, $\lambda = 150$, $t = 4.28$

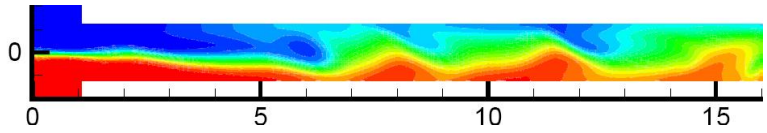

Figure 3.17 Plot of concentration, $\lambda = 150$, $t = 6.28$

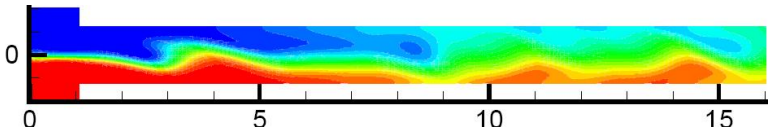

Figure 3.18 Plot of concentration, $\lambda = 150$, $t = 8.28$

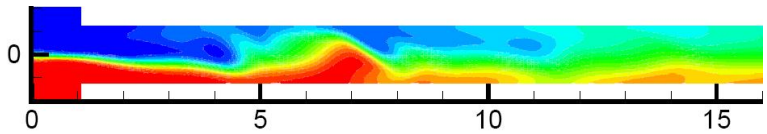

Figure 3.19 Plot of concentration, $\lambda = 150$, $t = 10.28$

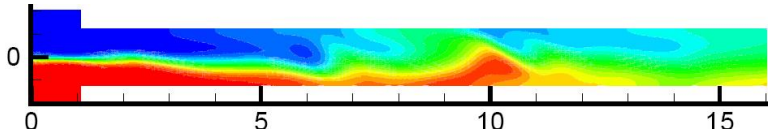

Figure 3.20 Plot of concentration, $\lambda = 150$, $t = 12.28$

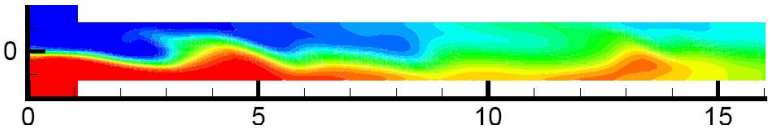

Figure 3.21 Plot of concentration, $\lambda = 150$, $t = 14.28$

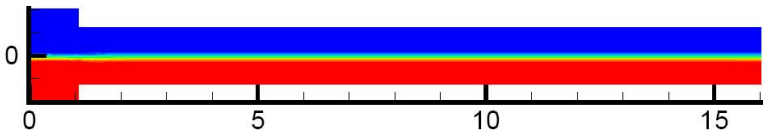

Figure 3.22 Plot of concentration, $\lambda = 180$, $t = 0.28$

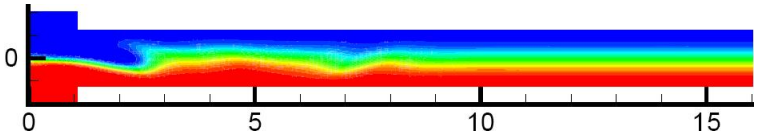

Figure 3.23 Plot of concentration, $\lambda = 180$, $t = 2.28$

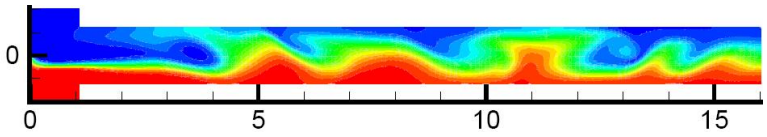

Figure 3.24 Plot of concentration, $\lambda = 180$, $t = 4.28$

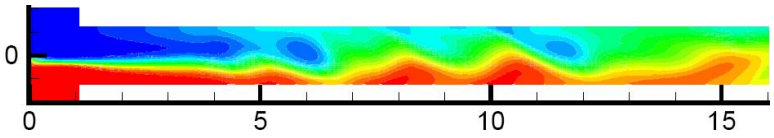

Figure 3.25 Plot of concentration, $\lambda = 180$, $t = 6.28$

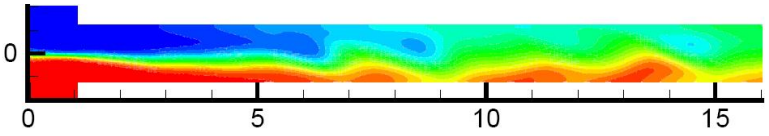

Figure 3.26 Plot of concentration, $\lambda = 180$, $t = 8.28$

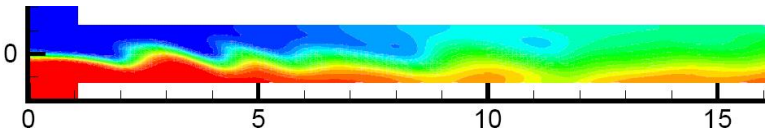

Figure 3.27 Plot of concentration, $\lambda = 180$, $t = 10.28$

3.2 Mixing Efficiency

In order to characterize mixing quantitatively, some notion of mixing effeciency is needed. Hu and Jin (2007) defined a mixing efficiency based on the intensity of pixels in the image. In this computational study, since the results of the entire flowfield are available, one can obtain a mixing efficiency on the entire flow field. Let c_h and c_l be the initial concentrations of the two mixing streams (called "high" and "low") respectively. Then the mixing efficiency is proposed as

$$ME(x, y, t) = \frac{4(c_h - c)(c - c_l)}{(c_h - c_l)^2} \tag{3.1}$$

where $c = c(x, y, t)$ is the instantaneous concentration at the point (x, y) at time t . Thus the mixing efficiency is 0 when there is no mixing (that is, when $c = c_h$ or $c = c_l$) and 1 when $c = \frac{c_h + c_l}{2}$.

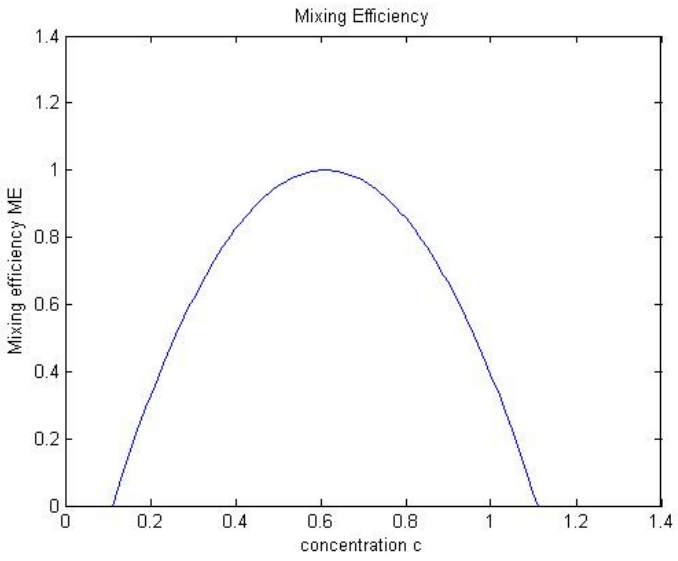

Figure 3.28 Plot of mixing efficiency as a function of increasing concentration

3.2.1 Mixing efficiency results for $\lambda = 160$

Reproduced below are the simulation results for $\lambda = 160$.

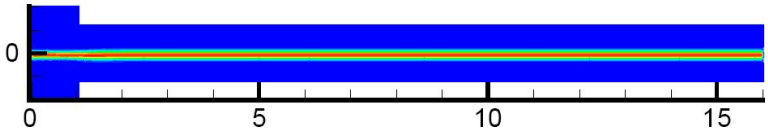

Figure 3.29 Plot of mixing efficiency, $\lambda = 160$, $t = 0.28$

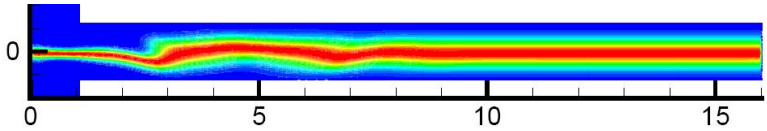

Figure 3.30 Plot of mixing efficiency, $\lambda = 160$, $t = 2.28$

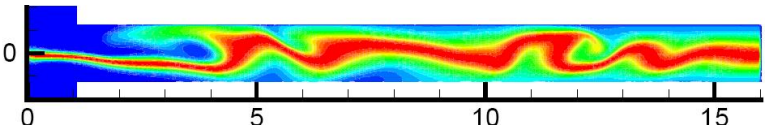

Figure 3.31 Plot of mixing efficiency, $\lambda = 160$, $t = 4.28$

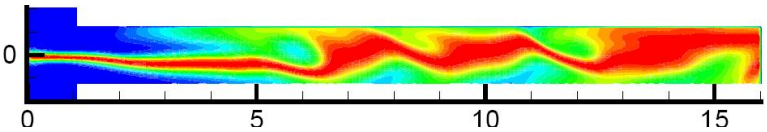

Figure 3.32 Plot of mixing efficiency, $\lambda = 160$, $t = 6.28$

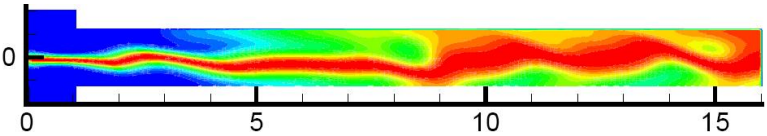

Figure 3.33 Plot of mixing efficiency, $\lambda = 160$, $t = 8.28$

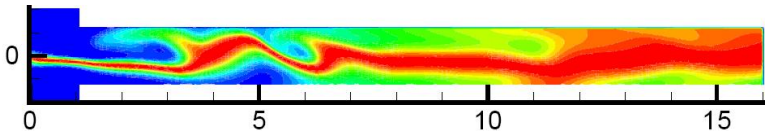

Figure 3.34 Plot of mixing efficiency, $\lambda = 160$, $t = 10.28$

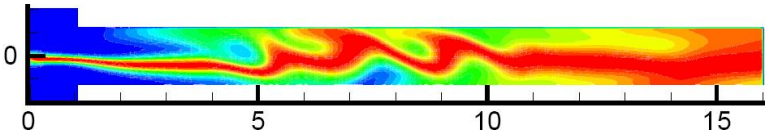

Figure 3.35 Plot of mixing efficiency, $\lambda = 160$, $t = 12.28$

3.2.2 Average Mixing Efficiency

The regions in red are those in which a lot of mixing has taken place and the blue regions are ones with very little mixing.

In order to compare the different cases with different values of λ the notion of average mixing efficiency is introduced as follows.

$$\overline{ME(x)} = \int_0^H \frac{ME(x,y)}{H} dy \tag{3.2}$$

where we integrate along the height of the channel to get the averaged mixing as a function of the x location.

It is quite instructive to plot the average mixing efficiency as a function of the distance x for different values of λ to obtain a quantitative estimate of the mixing.

Given below is such a plot where $\overline{ME(x)}$ has been plotted in the y axis and the distance x along the length of the channel is plotted in the x axis. $\overline{ME(x)}$ was averaged over a time period T for each of the different values of λ

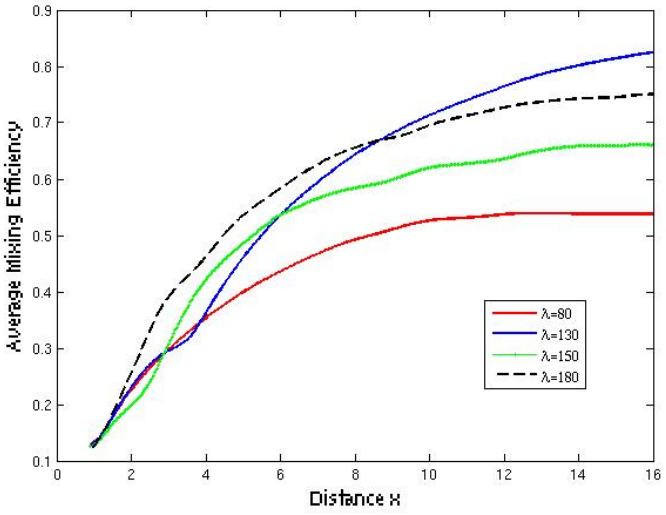

Figure 3.36 Average mixing efficiency along the length for different values of λ

As we can see from the figure, the mixing(as characterized by the formula above) is quite enhanced in the beginning portion of the t in the case where $\lambda = 180$ while it is attains the

maximum value for the case $\lambda = 130$ towards the end of the t.

3.3 Temporal evolution of the disturbance

Another interesting observation that has come up in this study is the observation that the time evolution of the disturbance is periodic. This was obtained by plotting the x velocity component at a monitoring point and observing how it changes with time. In every case of varying λ from 100 to 180 we could see that the disturbance was quite periodic. Also, for $\lambda = 80$ the disturbances died out due to viscous forces dominating as was also evident from the concentration plots shown earlier in this chapter. Based on this analysis, the critical value of λ is somewhere between 80 and 100 though it must be noted that finding the exact critical value of λ through these types of simulations is not feasible and one would have to resort to stability analysis.

The velocity of the monitoring point as it varies in time is plotted to obtain the natural period of the system. The plots are given below.

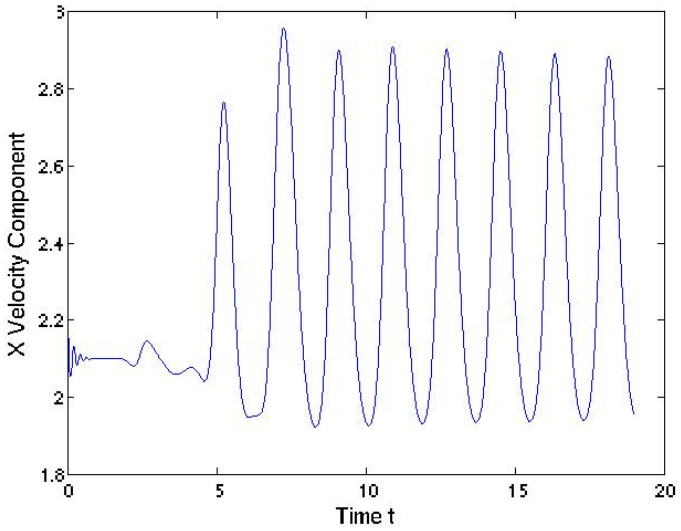

Figure 3.37 Velocity at monitoring point when $\lambda = 100$

The time periods for the different cases are computed and the result is plotted below giving the natural time period T of the system with respect to λ.

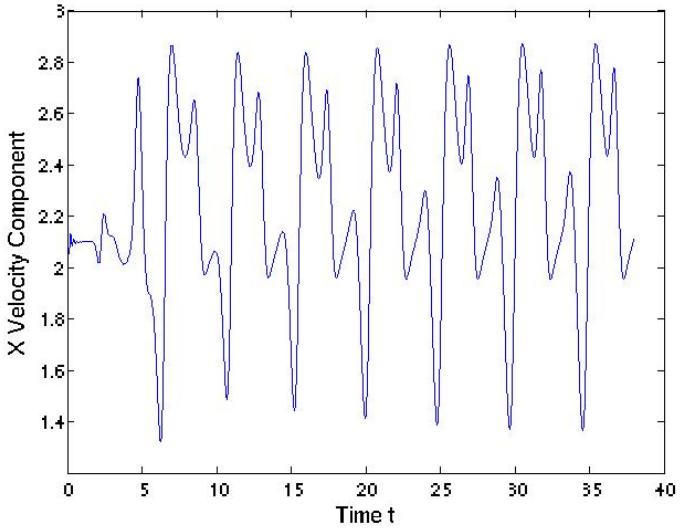

Figure 3.38 Velocity at monitoring point when $\lambda = 140$

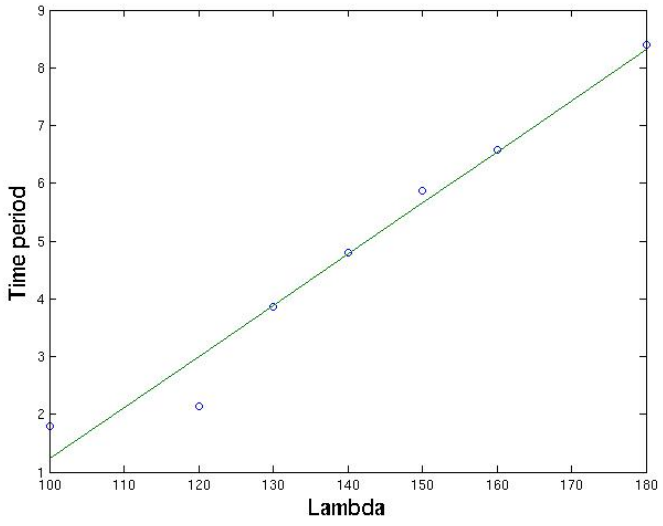

Figure 3.39 Variation of the Time period with increasing λ

λ	Time period
100	1.80
120	2.13
130	3.86
140	4.80
150	5.88
160	6.57
180	8.39

Table 3.1 Variation of Time period of disturbance with λ

3.4 Velocity plots

Given below are the plots of the velocity vectors for the case $\lambda = 180$. Although no attempt is made to analyse the physics behind the instability mechanisms it may yet be worthwhile to look at the vector plots to get a basic feel for the physics behind the instability and mixing. One can observe the formation of a strong counterclockwise vortex and its propogation downstream in agreement with the computer simulations of Kang *et al* (2006)

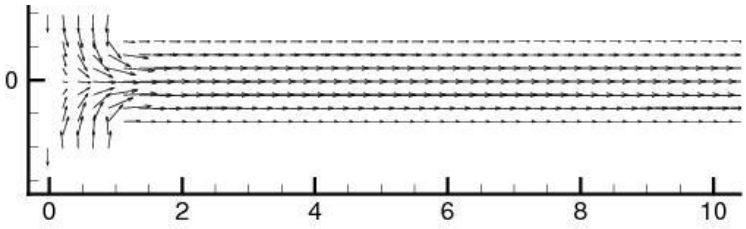

Figure 3.40 Plot of velocity vectors, $\lambda = 180$, $t = 0.28$

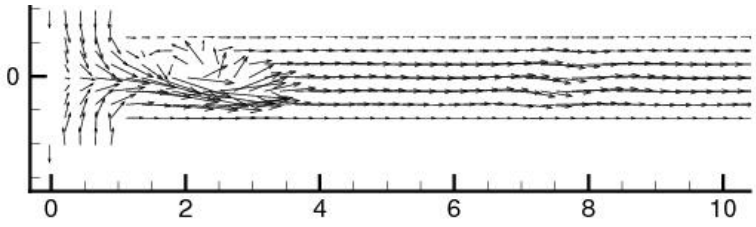

Figure 3.41 Plot of velocity vectors, $\lambda = 180$, $t = 2.28$

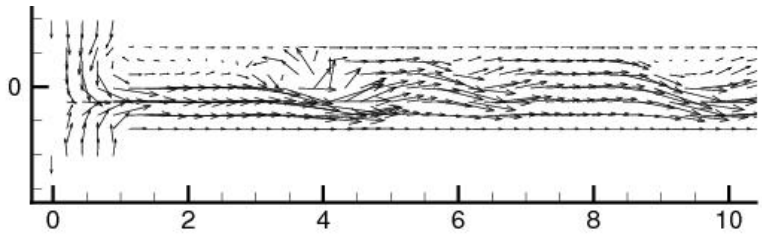

Figure 3.42 Plot of velocity vectors, $\lambda = 180$, $t = 4.28$

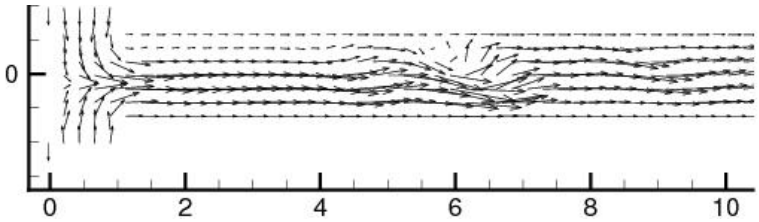

Figure 3.43 Plot of velocity vectors, $\lambda = 180$, $t = 6.28$

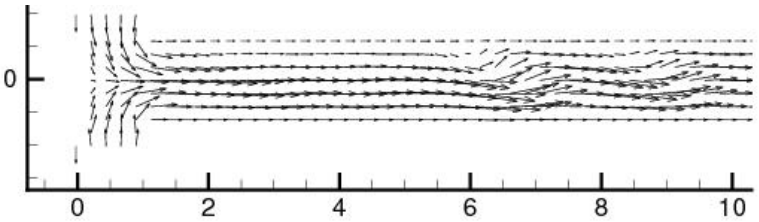

Figure 3.44 Plot of velocity vectors, $\lambda = 180$, $t = 8.28$

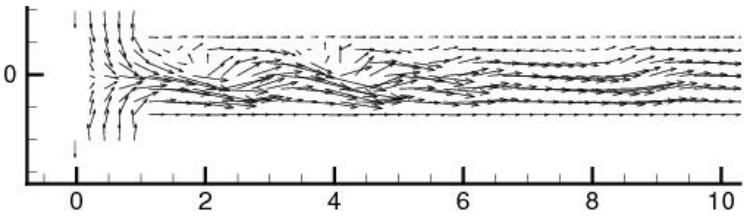

Figure 3.45 Plot of velocity vectors, $\lambda = 180$, $t = 10.28$

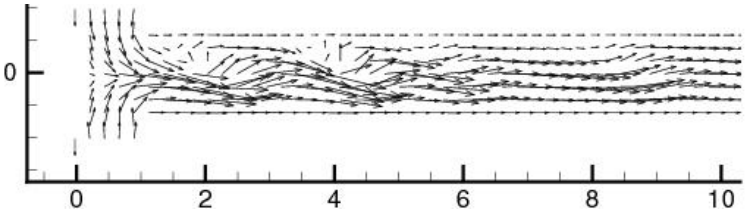

Figure 3.46 Plot of velocity vectors, $\lambda = 180$, $t = 12.28$

CHAPTER 4. RESULTS: CASE II: THE EFFECT OF FORCING

Having observed the mixing without any forcing, we would like to consider the case of forcing in order to see the effect it has on the mixing characteristics. Hu and Jin (2007) observed that maximum mixing can be achieved when the frequency of the external applied electric field is the same as the natural frequency of the system with no external forcing.

Let E_0 be the static electric field that is applied. In this simulation this applied electric field is replaed by $E_0 + 0.25E_0 \sin(\frac{2\pi t}{T})$ where T is the time period of the system without forcing that is obtained in the last chapter.(see Figure 3.39). The mixing efficiency is compared based on the two cases. The results obtained show that in the cases where $\lambda = 150, 160$ and 180 the mixing obtained is significantly larger than the case where there is no forcing in agreement with the general experimental observations of Hu and Jin (2007). In the case where $\lambda = 100, 120$ there is a marginal increse in the mixing efficiency and when $\lambda = 130$ the mixing efficiency actually is slightly below that of the unforced case.

4.1 Results of simulation with forcing

4.1.1 Case(i): $\lambda = 150$

Reproduced below are the results for this case. The interesting observation is that there is a lot more mixing in the forced case than there is in the unforced case. This is reinforced by plotting the mixing efficiency for the unforced and the forced case. It is quite evident from Figure 4.8 that there is significantly greater mixing by forcing at natural frequency compared to the case of the unforced system.

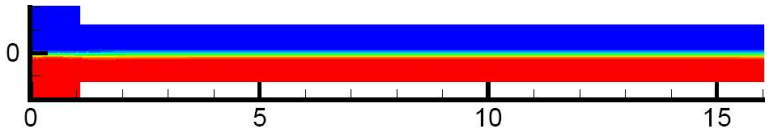

Figure 4.1 Plot of concentration with forcing at natural frequency, $\lambda = 150$, $t = 0.28$

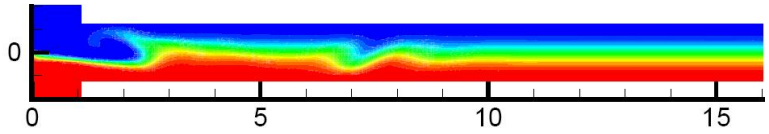

Figure 4.2 Plot of concentration with forcing at natural frequency, $\lambda = 150$, $t = 2.28$

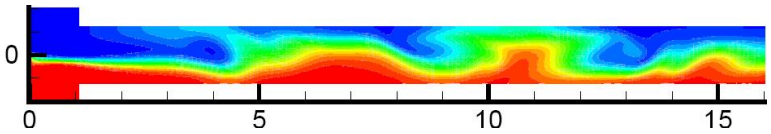

Figure 4.3 Plot of concentration with forcing at natural frequency, $\lambda = 150$, $t = 4.28$

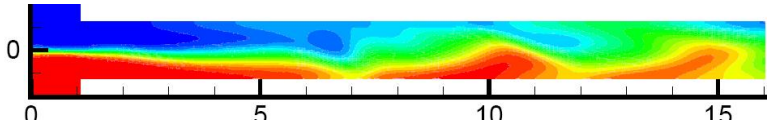

Figure 4.4 Plot of concentration with forcing at natural frequency, $\lambda = 150$, $t = 6.28$

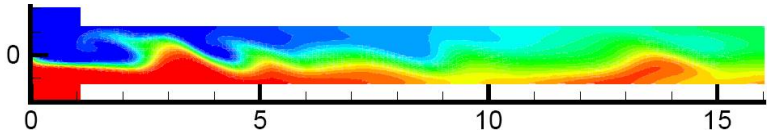

Figure 4.5 Plot of concentration with forcing at natural frequency, $\lambda = 150$, $t = 8.28$

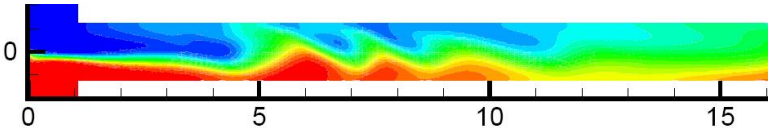

Figure 4.6 Plot of concentration with forcing at natural frequency, $\lambda = 150$, $t = 10.28$

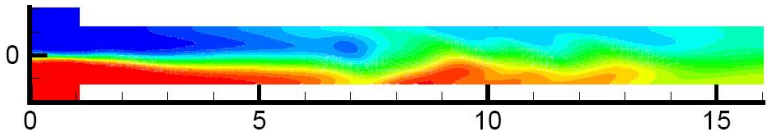

Figure 4.7 Plot of concentration with forcing at natural frequency, $\lambda = 150$, $t = 12.28$

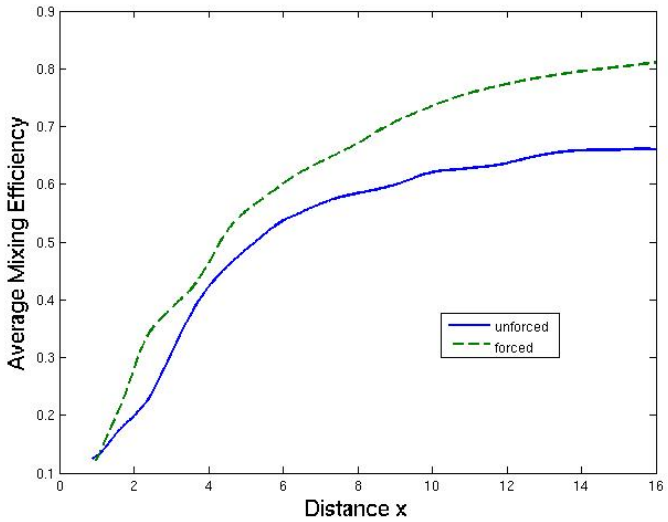

Figure 4.8 Comparison of mixing efficiency for forced and unforced cases, $\lambda = 150$

4.1.2 Case(ii): $\lambda = 180$

As in the previous case, in this case too, the mixing obtained is significantly more than in the unforced case. it can be seen that by the time $t = 6.28$, there is significantly large amounts of mixing compared to the previous case. This is evident from the mixing efficiency plotted below.

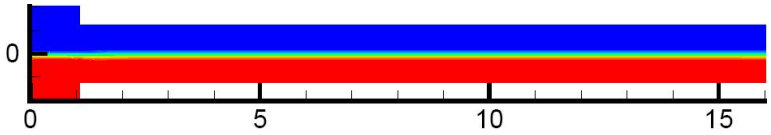

Figure 4.9 Plot of concentration with forcing at natural frequency, $\lambda = 180$, $t = 0.28$

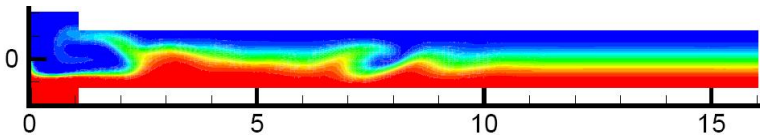

Figure 4.10 Plot of concentration with forcing at natural frequency, $\lambda = 180$, $t = 2.28$

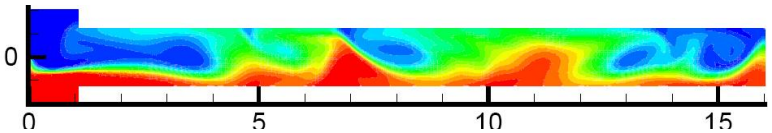

Figure 4.11 Plot of concentration with forcing at natural frequency, $\lambda = 180$, $t = 4.28$

4.1.3 Case(iii):$\lambda = 160$

For a different perspective, we plot the mixing efficiency for $\lambda = 160$ for the forced case and compare it with the unforced case. In this case too, the mixing obtained due to forcing is significantly greater than the mixing obtained without forcing.

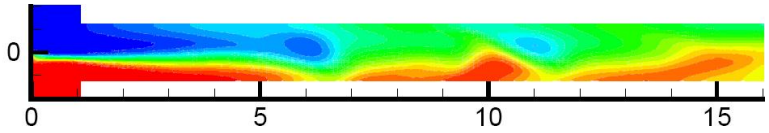

Figure 4.12 Plot of concentration with forcing at natural frequency, $\lambda = 180$, $t = 6.28$

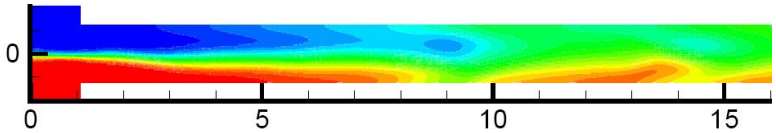

Figure 4.13 Plot of concentration with forcing at natural frequency, $\lambda = 180$, $t = 8.28$

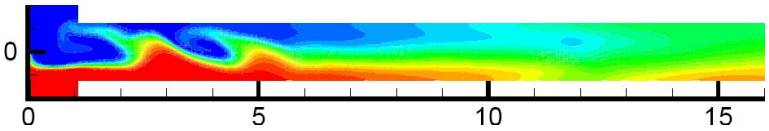

Figure 4.14 Plot of concentration with forcing at natural frequency, $\lambda = 180$, $t = 10.28$

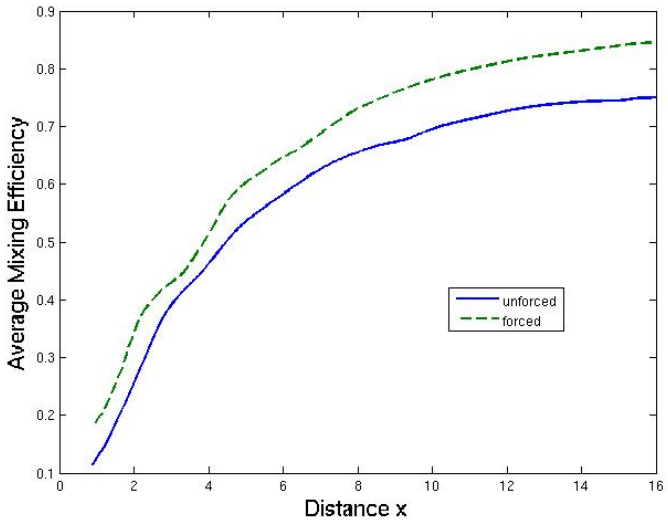

Figure 4.15 Comparison of mixing efficiency for forced and unforced cases, $\lambda = 180$

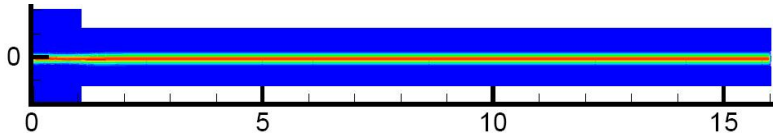

Figure 4.16 Plot of concentration with forcing at natural frequency, $\lambda = 160$, $t = 0.28$

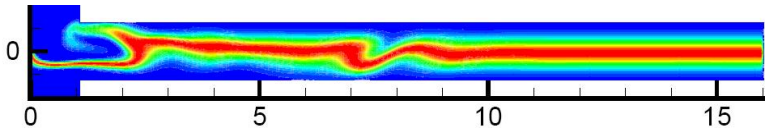

Figure 4.17 Plot of concentration with forcing at natural frequency, $\lambda = 160$, $t = 2.28$

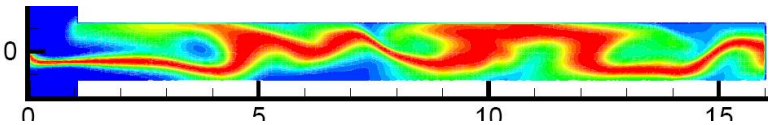

Figure 4.18 Plot of concentration with forcing at natural frequency, $\lambda = 160$, $t = 4.28$

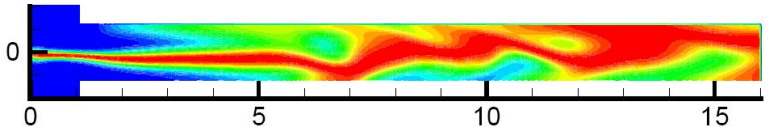

Figure 4.19 Plot of concentration with forcing at natural frequency, $\lambda = 160$, $t = 6.28$

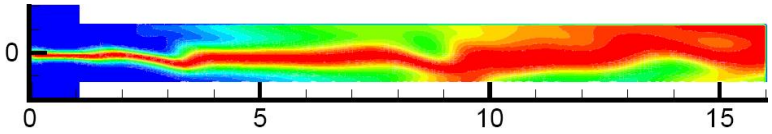

Figure 4.20 Plot of concentration with forcing at natural frequency, $\lambda = 160$, $t = 8.28$

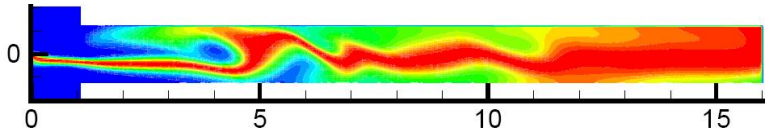

Figure 4.21 Plot of concentration with forcing at natural frequency, $\lambda = 160$, $t = 10.28$

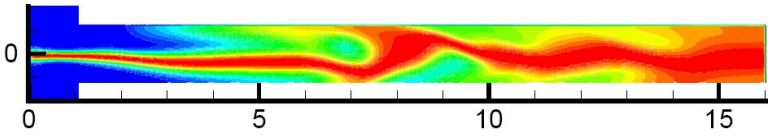

Figure 4.22 Plot of concentration with forcing at natural frequency, $\lambda = 160$, $t = 12.28$

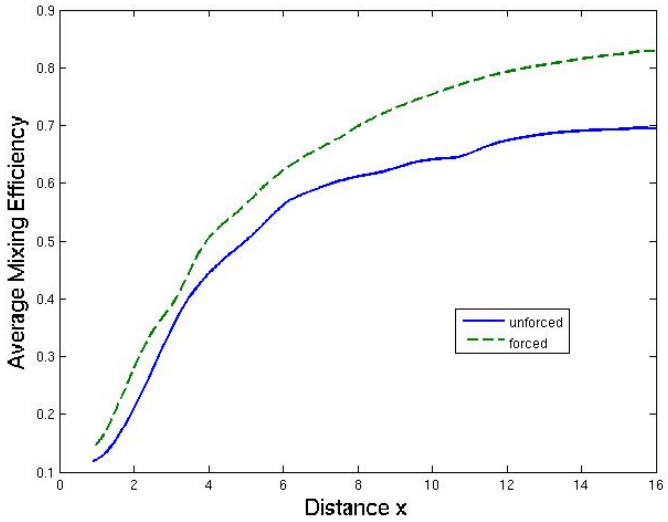

Figure 4.23 Comparison of mixing efficiency for forced and unforced cases, $\lambda = 160$

4.2 Average Mixing Efficiency with oscillation

It is also instructive to plot the mixing efficiencies with forcing for different values of λ. We can see from the plot below that the mixing efficiency is maximum for the case $\lambda = 180$ and increases with increasing value of λ. This result is in contrast to the unforced case where the maximum mixing efficiency was obtained for the case $\lambda = 130$. We can also see that in the case of $\lambda = 80$, there is much less mixing which shows that the mixing is due to the instability and not simply due to external forcing of the electric field. Simulations are also performed by oscillating the applied electric field at twice the frequency of the natural disturbance. Although the results are not presented here, it was observed that the effect on the mixing efficiency is very similar to the case of oscillating the electric field at the natural frequency. Thus, although oscillating the electric field at twice the natural frequency gives enhanced mixing compared to the case with no oscillation, the effect of oscillation at the natural frequency or twice the natural frequency seems to be quite the same.

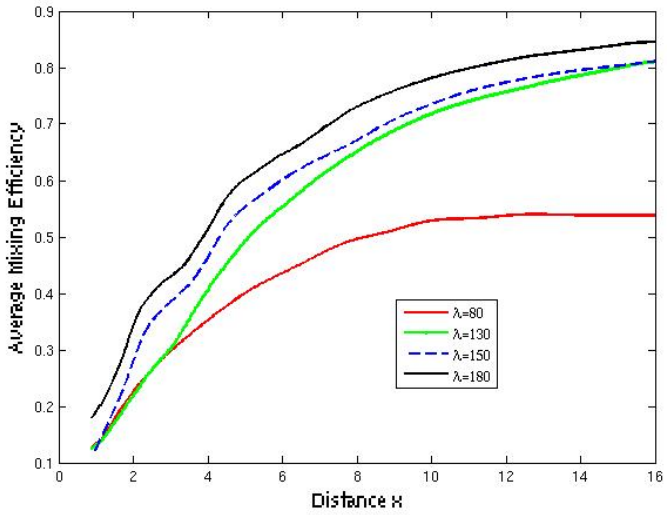

Figure 4.24 Average mixing efficiency along the length with forcing for different values of λ

CHAPTER 5. CONCLUSION

5.1 Summary

In order to understand the mixing characteristics of electrohydrodynamic flows in micro-scales, a computational study was performed in a t-shaped configuration with two streams having similar mechanical properties but differing in their electrical conductivities. The mixing was characterized in terms of a nondimensional number λ and the effect of varying this parameter on mixing was studied by means of computer simulations. A nondimensional mixing efficiency was proposed based on the relative concentrations of the two mixing streams and the mixing was quantitatively characterized based on this mixing efficiency. The conclusion was that in the case where there was no forcing, maximum mixing occured for the case when $\lambda = 130$ towards the downstream portion of the 't' channel. A surprising observation was that, for all the cases considered, varying from $\lambda = 80$ to $\lambda = 180$, the disturbance had a natural frequency associated with it and the time period of this disturbance was directly proportional to the value of λ. When the applied electric field was oscillated at the natural frequency of the disturbance, it was observed that there was significantly more mixing in the cases where $\lambda = 150, 160$ and 180 quite in agreement to the experimental observations of Hu and Jin (2007). In this case the mixing efficiency seemed to increase with increasing values of λ. Simulations were also performed by oscillating the applied electric field at twice the frequency of the natural disturbance. In this case the mixing efficiency was observed to be quite similar to the case of oscillating the electric field at the natural frequency. In the case of varying amplitude of the applied electric field, there is a marginal increase initially for increasing amplitude and then a significant increase when the amplitude of the applied field is about half the amplitude of the d.c. electric field which is also in agreement with the experimental

results of Hu and Jin (2007).

5.2 Suggestions for future work

One can continue this study in several different directions. Full scale three dimensional simulations can be performed instead of the present two dimensional simulations. One can also parallelize the code to obtain better computational performance. Methods from stability theory can be employed to better understand the instability mechanism and identify the physical mechanisms responsible for causing the instability. The present simulations were run for a fixed concentration ratio. One can do many simulations by varying different parameters and then perform an optimization study to find out how to maximize the mixing: either obtain mixing in even shorter length scales or obtain mixing faster in time.

BIBLIOGRAPHY

Baygents, J. C, Baldessari, F (1998). Electrohydrodynamic Instability in a thin fluid layer with an electrical conductivity gradient. *Physics of Fluids,* 10,301

Chen, C. H., Santiago,J. G.(2002) Electrokinetic instability in high concentration gradient microflows. *Proc. IMECE-2002* CD Vol.1, 33563

Chen, C-H, Lin,H., Lele, S.K., Santiago, J,G (2003). Electrokinetic microflow Instabilities with conductivity gradients *7th Int. Conf. Chem and Biochem Anal Sys, Squaw Valley, CA*pp-983-987

Chen, C-H, Lin,H., Lele, S.K., Santiago, J,G (2005). Convective and absolute electrokinetic instability with conductivity gradients. *Journal of Fluid Mechanics,* Vol 524, pp-263-303

Double layer (interfacial). (2009, February 19). In Wikipedia, the free encyclopedia. Retrieved February 19, 2009, from http://en.wikipedia.org/wiki/Double_layer_(interfacial)

Ferziger, J. H., Peric, M. (1994) Computational Methods for Fluid Dynamics, *Springer*

Ferziger, J. H., Peric, M. (1994) Computer Codes for Computational Methods for Fluid Dynamics, available at ftp://ftp.springer.de/pub/technik/peric/

Hoburg, J. F, Melcher, J. R (1976). Internal electrohydrodynamic instability and mixing of fluids with orthogonal field and conductivity gradients. *Journal of Fluid Mechanics,*Vol.73,part 2,

Hu, H., Jin, Z.,(2007). Fluid mixing control inside a Y-shaped microchannel by using electrokinetic instability *Proc. of FEDSM07*

Kang, K. H, Park, J.,Kang, I. S.,Huh,K. Y(2006). Initial growth of electrohydrodynamic instability of two-layered miscible fluids in T-shaped microchannels. *International Journal of Heat and Mass Transfer,* 49, pp-4577-4583

Lin, H., Storey, B. D., Oddy, M. H., Chen, C-H., Santiago, J. G(2004). Instability of electrokinetic microchannel flows with conductivity gradients. *Physics of Fluids,* 16, pp 1922-1935

Oddy, M. H.,(2005). Electrokinetic Transport Phenomena:Mobility measurement and Electrokinetic Instability. PhD Thesis, Stanford University.

Park, J., Shin, S. M., Huh, K. Y, Kang, I. S(2005) Application of electrokinet ic instability for enhanced mixing in various micro- T-channel geometries. *Physics of Fluids,* 17, 118101

Patankar,S. V., (1980) Numerical Heat transfer and Fluid Flow, *Taylor and Francis*

Probstein, R. F. (1994). Physicochemical Hydrodynamics *John Wiley and Sons Inc*,

Rhie, C. M., Chow, W. L.,(1983). A numerical study of the turbulent flow past an isolated airfoil with trailing edge separation. *AIAA J.* 21, pp 1525-1532

Saville, D. A, (1998). Electrohydrodynamics: The Taylor-Melcher leaky dielectric model. *Annual Review of Fluid Mechanics,* 29,27-64

Stone, H. L., (1968). Iterative solution of implicit approximations of multidimensional partial differential equations. *SIAM J. Numer Anal.* 5, pp 530-558

Taylor, G. I. , Melcher, J. R (1969). Electrohydrodynamics: A Review of the Role of Interfacial Shear Stresses. *Annual Review of Fluid Mechanics,* Vol.1,